EFFECTS OF NOZZLE GEOMETRY ON SF_6 ARC THERMAL INTERRUPTION

Q. ZHANG, J. D. YAN* AND M. T. C. FANG

Department of Electrical Engineering and Electronics, University of Liverpool, Liverpool, L69 3GJ, UK
*email: yaneee@liv.ac.uk

ABSTRACT

The effects of nozzle geometry on SF_6 arc thermal interruption are investigated using the Prandtl mixing length model. The measured and computed RRRV for three different nozzles are used to evaluate the influence of nozzle geometry on turbulence level.

1. INTRODUCTION

Supersonic nozzle interrupters are commonly used in modern gas blast circuit breakers for the control of arc discharge conditions [1]. It is well-known that turbulent energy transport plays a critical role in thermal extinction of an SF_6 nozzle arc [2]. Nozzle geometry determines the flow conditions, hence the turbulence level in the current zero period. Optimization of the nozzle interrupter is therefore an important part in the design process of a circuit breaker.

Of the commonly used turbulence models the Prandtl mixing length model gives overall better prediction of SF_6 arc behaviour during the current zero period [3]. The purpose of the present investigation is to use the Prandtl mixing length model to study the effects of nozzle geometry on the turbulence level during the current zero period. The measured critical rate of rise of recovery voltage (RRRV) for three nozzles [1, 4, 5] together with the computational results will be used to evaluate the level of turbulence and the influence of the geometrical factors of a nozzle on thermal interruption.

2. NOZZLE GEOMETRIES

The three nozzle-electrode configurations used in the current investigation are respectively those of GE [4, 5] (Nozzles 1 and 2) and that of Frind and Rich [1] (Nozzle 3), which are shown in Fig. 1. Z=0 indicates the axial position of the nozzle throat. These nozzles have the same expansion half angle (15 °) but differ in upstream and throat regions. The diameter of Nozzle 2 is twice that of Nozzle 1. Nozzle 3 is almost the same as Nozzle 2 except that the area variation of Nozzle 3 is continuous.

Experiments on the three nozzles [1, 4, 5] were not designed to study specifically the effects of nozzle geometry because the shapes of the upstream electrodes and the locations of the electrode tip are different. Because of these differences the arc lengths before nozzle throat are different for the three nozzles. Flow before the nozzle throat can also be affected by the upstream electrode. Since the critical arc section for arc interruption is downstream the nozzle throat [2, 6], differences in upstream electrode configurations are not expected to substantially affect the RRRV. We therefore attribute the differences in RRRV for the three nozzles to the influence of nozzle geometry. The arc lengths for Nozzles 1 and 2 are almost the same, 20mm. For Nozzle 3 the arc is 50 mm long.

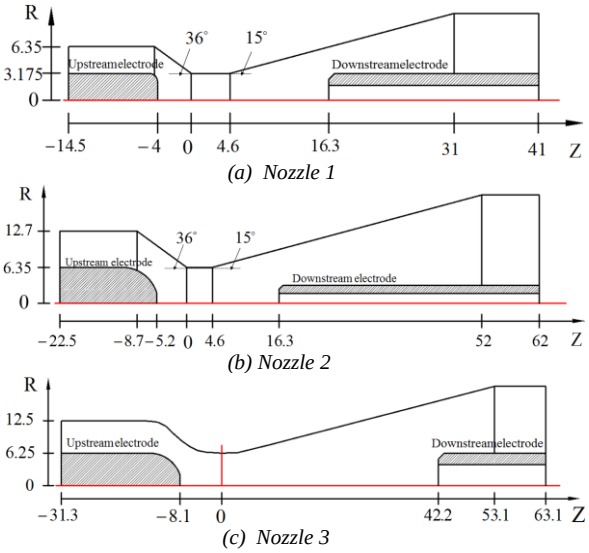

Fig.1 Nozzle geometries. Unit of nozzle dimensions: mm.

3. THE GOVERNING EQUATIONS

By assuming local thermal dynamic equilibrium (LTE) the behaviour of the arc and its surrounding flow is determined by the time-averaged Navier-Stokes equations:

$$\frac{\partial(\rho\phi)}{\partial t}+\frac{1}{r}\frac{\partial}{\partial r}\left[r\rho v\phi - r\Gamma_\phi\frac{\partial\phi}{\partial r}\right]+\frac{\partial}{\partial z}\left[\rho w\phi-\Gamma_\phi\frac{\partial\phi}{\partial z}\right]=S_\phi \quad (1)$$

where ρ is the gas density, v and w the radial and axial velocity components, and ϕ is the dependent variable which is 1 for the continuity equation, v and w respectively for the radial and axial momentum equations, and h for the energy equation. The source terms (S_ϕ) and diffusion coefficients (Γ_ϕ) for different conservation equations are detailed in [6].

The axial electrical field (E) is calculated by the simplified Ohmic law

$$E = i\Big/\int_0^\infty \sigma 2\pi r dr \quad (2)$$

where σ is the electrical conductivity.

Turbulent eddy viscosity is given by

$$\mu_t = \rho\ell_m^2\left(\left|\partial w/\partial r\right|+\left|\partial v/\partial z\right|\right) \quad (3)$$

where the length scale is related to the arc thermal radius through a turbulence parameter, c, which yields

$$\ell_m = c\sqrt{\int_0^\infty \left(1-T_\infty/T\right)\cdot 2r dr} \quad (4)$$

4. RESULTS AND DISCUSSIONS

Version 3.6.1 of PHOENICS has been used to obtain the results. Computations were carried out using a current ramp with a plateau of 1 kA and a rate of current decay, di/dt, before current zero and voltage ramp (dV/dt) after current zero to determine the RRRV. The boundary conditions for Equation (1) are the same as those given in [6]. The stagnation pressure (P_0) for Nozzles 1 and 2 is 35 atm (absolute) and di/dt=25 A/μs with an exit pressure (P_e) to ensure shock free in the nozzle. For Nozzle 3, P_0=37.5 atm, di/dt= 27 A/μs and $P_e=P_0/4$.

The turbulence parameter, c, was adjusted to give the closest agreement between the computed and measured RRRV. The values of c for the three nozzles and the computed RRRV are given in Table 1. Influences of the nozzle geometry on the gas flow and energy transports of the arc will be discussed below.

Table 1. Turbulence parameters c and computed RRRV for different nozzles

	c	RRRV (kV/ μs)
Nozzle 1	0.053	6.5
Nozzle 2	0.048	7.85
Nozzle 3	0.045	2.83

Axial variations of axis pressure and velocity at 1 kA DC and at current zero for the three nozzles are shown in Figs. 2 and 3. There is a shock in Nozzle 3, the location of which almost coincides with the position of the downstream electrode tip in Nozzles 1 and 2. The voltage taken up by the arc section behind the shock accounts for less than 20% of the total arc voltage before current zero and is negligible a few microseconds before current zero [6]. This makes the effective arc length of Nozzle 3 for arc interruption the same as those in Nozzles 1 and 2. This renders the use of RRRV for the three nozzles as a means to assess the turbulence effects meaningful.

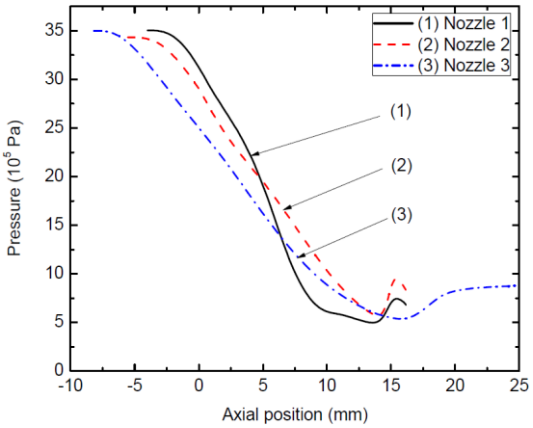

(a) 1 kA DC

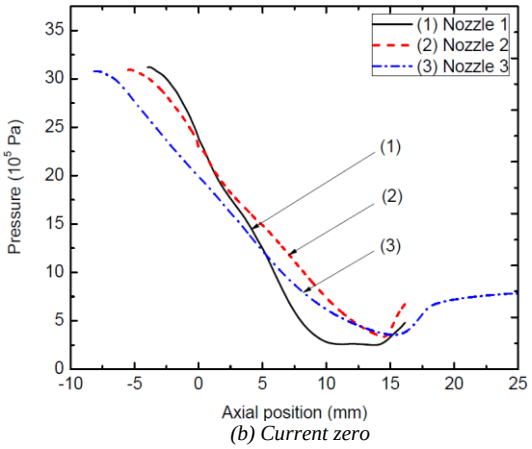

(b) Current zero

Fig. 2. Variations of pressure along the nozzle axis

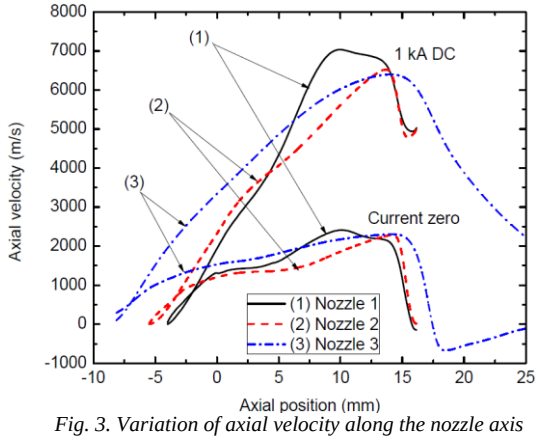

Fig. 3. Variation of axial velocity along the nozzle axis

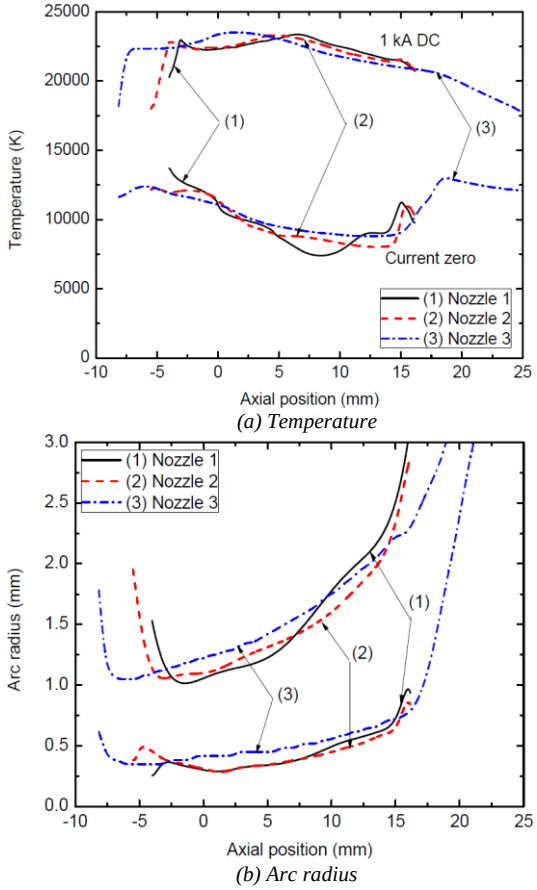

(a) Temperature

(b) Arc radius

Fig. 4 Axis temperature and arc radius for the three nozzles

For a given stagnation pressure and in the absence of a sizeable upstream electrode the axial variation of nozzle area ratio (nozzle area/throat area=A/A_t) approximately determines pressure distribution within the nozzle. Axial pressure gradient controls the axial growth of the arc radius through enthalpy transport while the absolute value of pressure determines the radiation loss. Thus, optimization of nozzle geometry can achieve the best interruption performance by controlling arc temperature and radius.

Nozzles 1 and 2 have the same stagnation pressure but the mass flow rate of Nozzle 2 is approximately 4 times that of Nozzle 1. Compared with Nozzle 1, Nozzle 2 has a gentler area variation, which results in a slower rate of pressure decrease than Nozzle 1 (Fig. 2). Thus, gas acceleration in Nozzle 1 is stronger than Nozzle 2 (Fig. 3). The arc radius of Nozzle 1 is smaller in the region where Z<7.5mm than that of Nozzle 2 but the reduction in absolute pressure after Z=7.5mm makes the arc radius larger than that of Nozzle 2 both at 1 kA and at current zero (Fig. 4b). Nozzles 2 and 3 have the same throat area with slightly different stagnation pressures, thus nearly the same mass flow rate. Nozzle 3 gives the smallest axial pressure gradient (dp/dz) as well as the lowest absolute pressure (Fig. 2) for the major part of its length. The arc radius for Nozzle 3 is therefore the largest (Fig. 4b). Thus, of the three nozzles, for the arc radius averaged over the whole arc length Nozzle 2 has the smallest arc radius.

It has been found that when an arc is in quasi-steady state, around 90% of the current is carried by a high temperature core, the boundary of which is defined by 83% of the axis temperature [7]. Arc voltage is determined by the energy balance of this high temperature core. Energy balance calculations for the three nozzles show that Ohmic input into this core is largely taken out by radiation. For such radiation transport dominated arc core the axis temperature is not sensitive to nozzle geometry (1 kA curves in Fig. 4a) and the arc voltage for a given nozzle is almost independent of current for current greater than 600 A (Fig. 5). When the current decays towards its zero point, the arc column contracts which favours radial turbulent thermal conduction. Turbulent thermal conduction gradually becomes the dominant energy loss mechanism and arc voltage starts to rise. Thus, the accumulated turbulence effects determine the axis temperature and arc radius at current zero. These two quantities give a very good indication regarding the relative magnitudes of RRRV for the three nozzles. The axis temperature and arc radius in Fig. 4 indicates that Nozzle 2 will give the highest RRRV.

The value of the turbulence parameter, *c*, is not a good indicator of turbulence level as turbulence length scales for the three nozzles are different. In addition to the axis temperature and arc radius at current zero, arc voltage before the current

zero point is the most sensitive indicator regarding the accumulated effects of turbulence cooling. As shown in Fig. 5, when the current is high (i > 100 A) Nozzle 3 gives the highest arc voltage due to its arc length being 2.5 times larger than those of Nozzles 1 and 2. However, when current zero is approached, the effective arc length of Nozzle 3 becomes the same as those of the other two nozzles. The arc voltage for Nozzle 3 is the lowest towards current zero (Fig. 6). Since during current zero period turbulence cooling is the most important energy transport mechanism, the highest extinction peak of Nozzle 2 (Figs. 5 and 6) indicates that the highest turbulence level is attained within Nozzle 2.

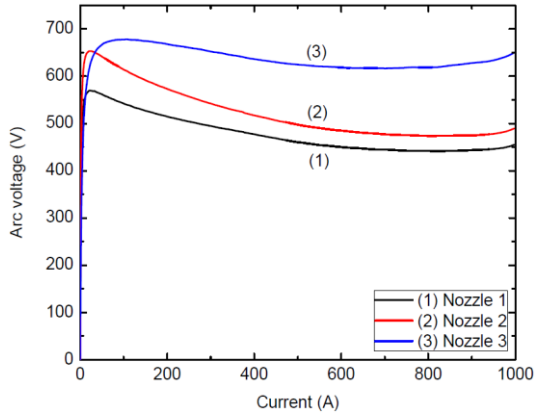

Fig. 5. Voltage-current characteristics for the arcs in the three nozzles

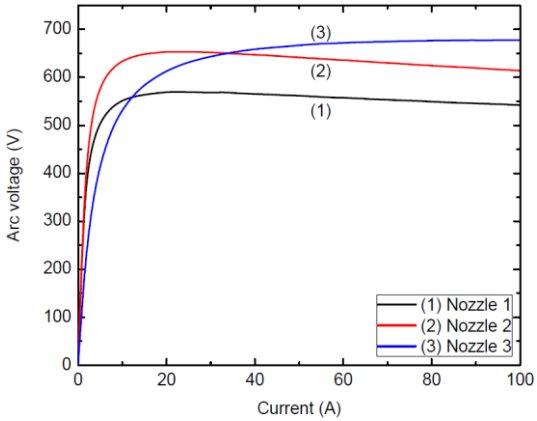

Fig. 6. Enlarged voltage-current characteristics in the last 4 mircoseconds before current zero.

4. CONCLUSIONS

The effects of nozzle geometry on SF_6 arc thermal interruption are investigated using the Prandtl mixing length model. The measured and computed RRRV for three different nozzles are used to evaluate the influence of nozzle geometry on turbulence level.

Nozzle geometry together with the stagnation pressure controls dp/dz and the absolute value of pressure within the nozzle. The effects of nozzle geometry on turbulence are studied under the condition of nearly identical stagnation pressures for three different nozzles. The pressure distribution of Nozzle 2 ensures (Fig. 2) the strongest accumulated turbulence cooling during current zero period. In this sense the geometry of Nozzle 2 is preferred. However, the running cost of a circuit breaker based on Nozzle 2 will be higher than Nozzle 1 as the required amount of SF_6 for Nozzle 2 will be much more than that needed for Nozzle 1. In terms of RRRV per unit mass flow rate the performance of Nozzle 1 is the best. In order to raise RRRV while keeping the same mass flow rate for Nozzle 1, we should reduce the expansion half angle to increase the absolute pressure in the divergent section of Nozzle 1. Such work is currently in progress.

REFERENCES

[1] G. Frind and J. A. Rich, "Recovery speed of axial flow gas-blast interrupter: dependence on pressure and di/dt for air and SF_6", IEEE Trans. Power Appar, Syst. **93**, pp. 1675-84, 1974.

[2] M. T. C. Fang, Q. Zhuang, X. J. Guo, "Current-zero behaviour of an SF6 gas-blast arc. Part II: turbulent flow", J. Phys. D: Appl. Phys. **27**, pp. 74-83, 1994.

[3] Q. Zhang, J. D. Yan and M. T. C. Fang, "Modelling of turbulent arc burning in a supersonic nozzle", Proc. Int. Conf. on Gas Discharges and Their Applications. pp. 202-205, 2012.

[4] G. Frind, R. E. Kinsinger, R. D. Miller, H. T. Nagamatsu and H. O. Noeske, "Fundamental investigation of arc interruption in gas flows EPRI EL-284 (Project 246-1)", January, 1977.

[5] D. M. Benenson, G. Frind, R. E. Kinsinger, H. T. Nagamatsu , H. O. Noeske and R. E. Sheer, Jr, "Fundamental investigation of arc interruption in gas flows EPRI EL-1455 (Project 246-2)", July, 1980.

[6] Q. Zhang, J. D. Yan and M. T. C. Fang, "Current zero behaviour of an SF_6 nozzle arc under shock conditions", J. Phys. D: Appl. Phys. **46**, 165203, 2013.

[7] Q. Zhang, J. D. Yan and M. T. C. Fang, "Modelling of SF_6 arc in a supersonic nozzle. Part I: cold flow features and DC arc characteristics", submitted to J. Phys. D: Appl. Phys. 2014.